Suppression of Cavitation Surge in Turbopump with Inducer by Reduced-Diameter Suction Pipe with Swirl Brake

Tanaka, Yohei
Graduate School of Engineering, Kyushu University

Kitabata, Takahiro
Graduate School of Engineering, Kyushu University

Nasu, Koichi
Graduate School of Engineering, Kyushu University

Watanabe, Satoshi
Department of Mechanical Engineering, Faculty of Engineering, Kyushu University

他

https://hdl.handle.net/2324/4787581

American Society of Mechanical Engineers

ASME Accepted Manuscript Repository

Suppression of Cavitation Surge in Turbopump with Inducer
by Reduced-Diameter Suction Pipe with Swirl Brake

Yohei Tanaka
Graduate School of Engineering, Kyushu University
744 Motooka, Nishi-ku, Fukuoka 819-0395, Japan

Takahiro Kitabata
Graduate School of Engineering, Kyushu University
744 Motooka, Nishi-ku, Fukuoka 819-0395, Japan

Koichi Nasu
Graduate School of Engineering, Kyushu University
744 Motooka, Nishi-ku, Fukuoka 819-0395, Japan

Watanabe, Satoshi[1]
Department of Mechanical Engineering, Faculty of Engineering, Kyushu University
744 Motooka, Nishi-ku, Fukuoka 819-0395, Japan
fmnabe@mech.kyushu-u.ac.jp
ASME Membership: #000004595914

Akira Sakata
IHI Corporation
3975-18 Haijima-cho, Akishima, Tokyo, 196-8686, Japan

ABSTRACT

Downsizing and high power density of turbopumps are achieved by increasing their rotational speed. Cavitation often becomes a problem while the influence of cavitation will be generally relieved by employing an inducer before the impeller. For general-use turbopumps with inducer, instability-free operation as well as high suction performance are required in wide flow rate range including extremely low flow rate. However, the low frequency and large amplitude of cavitation surge is often to be a serious problem even with inducer when operated at very low flow rates. In this study, a reduced-diameter suction pipe (RSP) equipped with

swirl brake (SB) was proposed for a suppression device of the inlet backflow as well as of the cavitation surge through removing swirling velocity component. The effectiveness of this device was investigated by CFD and experiments. First, several geometries of RSP with SB were examined by CFD, and it was found that the extension of inlet backflow was stopped at this device provided that the swirl brake had a sufficient radial or axial length. Then, one of the proposed RSP with SB was manufactured, and the experimental evaluation of the effectiveness of this device was conducted. It seemed that RSP with SB could well prevent the extension of inlet backflow. The cavitation surge was completely suppressed even at extremely low flow rates. As a result, the suction performance was also improved at low flow rates.

INTRODUCTION

Downsizing and high power density of turbopumps are achieved by increasing their rotational speed. However, with high rotational speed, the local pressure especially around the pump impeller can be significantly lower than the suction pressure, and then a phase change phenomenon, namely cavitation, occurs if the local pressure falls below vapor pressure. The occurrence of cavitation generally leads to the various problems such as a deterioration of pump performance, machine vibrations and noises, material damages (cavitation erosion) and etc. Installing an inducer upstream of the impeller is known to be one of the effective ways to improve the suction performance of pumps, since inducers can produce the head rise even in severely cavitating conditions because of their geometrical features; large inlet passage area, axial or mixed flow type meridional passage, long blades (large solidity) and so on [1]. However, cavitating inducers often suffer from so called cavitation instabilities such as rotating cavitation and cavitation surge [2]-[5] which limit the safe operation of pumps. The operation range of commercial turbopumps often extends from shut-off to over flow rate. Therefore, considering the application of inducer for such pumps to enhance the suction performance, it is apparently important to understand the mechanism of cavitation instabilities and to develop the suppression methods applicable for the wide flow rate range.

The onset mechanism of cavitation instabilities can be well explained by using cavitation characteristics of pumps, cavitation compliance and mass flow gain factor, which appear in a dynamic transfer matrix of pumps [6]. Tsujimoto et al. [7] have found that the rotating cavitation, a two-dimensional rotating phenomenon around impeller, is caused by a positive mass flow gain factor, the increase of cavity volume against the increase of incidence angle. They have also shown that there can exist two modes, forward and backward rotating modes, while the former is more

commonly observed in experiments. Tsujimoto et al. [8] well summarize the cavitation instabilities of pumps, rotating cavitation and cavitation surge, with clear comparisons to the well-known performance-related instabilities in pumping system, rotating stall and surge. Recently, Watanabe and Tsujimoto [9] have introduced the idea of phase lags of cavity volume response against flow disturbances and have succeeded in well explaining the onset range of cavitation surge. On the other hand, there are several efforts to explain the onset mechanism of cavitation instabilities in more phenomenological ways. Watanabe et al. conducted a two-dimensional singularity analysis for a flat plate cascade using free streamline theory with a thin closed partial cavity, and firstly succeeded in simulating rotating cavitation [10] and cavitation surge [11] without using any tuning parameters nor experimental data. It has been found that the cavitation instabilities occur when the cavity trailing edge approaches to the throat of the blade passage, at which the cavity tailing edge begins to interact the flow around the leading edge of next blade. Although the main portion of cavitation of actual inducer is often in tip leakage vortices, Kang et al. [12] have observed the similar interaction at the onset of rotating cavitation. They also examined the effect of inducer blade design on the cavitation instabilities and found some guideline to avoid their occurrences.

Since it is generally difficult to avoid cavitation instabilities in the operation range only by the blade design, there have been several suppression methods/devices proposed in past literature. Kamijo et al. [13] applied a slight modification of upstream housing of inducer, i.e., slightly enlarged diameter than that of cylindrical part around inducer, to suppress rotating cavitation in H-II rocket engine LOX turbopump. Because of easy implementation of this method, it seems to be a common one in modern rocket engine turbopumps. To enlarge the range of operation flow rate of inducer, various kinds of casing treatments such as J-Groove [14], circumferential groove [15] and backflow restriction step [16] have been proposed and have contributed to extend our

knowledge in terms of the suppression of cavitation instabilities. However, the effectiveness of them were examined in the limited range of the flow rate, from slightly partial flow rate to the design or over flow rate, and some of them seem to be not effective at extremely low flow rates, at which a large flow recirculation due to strong inlet backflow from inducer occurs in nature [17]. At such low flow rates, it is well known that a violent cavitation surge with huge amplitude and low frequency occurs in cavitating pumps and inducers [18]. Since this phenomenon occurs associated with the large flow recirculation at the inlet originated from the backflow from rotating impeller, it is hardly avoided by usual suppression devices which only locally control the flow around the impeller. Sloteman et al. [19] proposed the backflow re-circulator (BFR) (recently refereed as stability control device [20]) as a powerful device to suppress the cavitation surge. The flow is well regulated by BFR with collecting the swirling backflow from the impeller, deswirling it and then returning to the main flow far upstream of pump through the external flow passage. As a result, the flow recirculation is totally removed. As a simpler device, a ring-shaped obstacle plate like orifice plate [21] and a reduced-diameter suction pipe (slightly smaller suction pipe than inducer tip diameter) [22] were proposed with the idea of stopping the backflow by some of the present authors. However, it was confirmed that the suppression effect of cavitation surge was insufficient at extremely low flow rates, at which the inlet backflow extends over the device and the large flow recirculation finally forms.

In the present study, for further suppression of inlet backflow and cavitation surge, we propose a new simple suppression device. We add a swirl brake similar to that proposed by Tsubouchi et al. [23] onto the reduced-diameter suction pipe [22] to remove the swirling velocity of the backflow from the impeller. To confirm the effect of this new device on the inlet backflow and the flow recirculation, computational fluid dynamics (CFD) simulation is firstly conducted. A

model inducer with simpler geometry which was used in our previous investigation on the inducer design [24] is utilized for the numerical investigation. In addition to flow features including the magnitude of flow recirculation, suction performance of the model inducer is investigated by employing a homogeneous cavitation model proposed by Zwart et al. [25]. Then the basic geometrical parameters of suppression device are determined and manufactured for the experimental investigation. The experiment is conducted at a closed test loop in Kyushu University. A turbopump consisting of a main impeller and a typical inducer employed in our previous investigation [26] is used to examine the effect of new suppression device on flow instabilities. The full onset map of instabilities is finally obtained, showing the excellent suppression ability of the proposed device.

NUMERICAL INVESTIGATION

Inducer Model and Inlet Geometries with Suppression devices

Figure 1 and Table 1 respectively show the schematic view and specifications of inducer used in this numerical investigation. This inducer was used in our previous investigation on the inducer design and was called "Non-splitter inducer" [24]. The occurrence of cavitation surge has been confirmed at low flow rates. It should be noted that this inducer does not have a sweptback leading edge, and this simplified geometry enables an easier construction of the numerical model and the computational mesh. In this section, by using this model inducer, the several devices are modeled to examine their suppression capability of the inlet backflow which seems to be in close relation to the occurrence of cavitation surge.

Figure 2 shows the schematic views of suppression devices of inlet backflow examined in the present investigation. Figure 2 (a) shows a circumferential groove combined with swirl brake (SB) which is designed on the basis of the investigation made by Tsubouchi et al [23]. The radial

depth δ and the axial width w of the groove are $0.07D_t$ and $0.20D_t$ respectively, where D_t is the tip diameter of the inducer. The SB is composed of 24 protuberances which are circumferentially equally distributed on the upstream wall of the groove. The axial height and the circumferential width of protuberance are both $0.02D_t$. Figure 2 (b) shows a reduced-diameter suction pipe (RSP) with the inner diameter of $D' = 0.78D_c$, where D_c is the casing diameter ($D_c = D_t + c$, c: tip clearance). The connected location L of RSP is $0.30D_t$ upstream from the inducer leading edge location. The RSP with $D' = 0.89D_c$ is also examined to see the effect of the inner diameter ratio D'/D_c on the suppression capability of the inlet backflow. Figure 2 (c) shows the RSP of $D' = 0.78D_c$ with swirl brake (SB). Similarly to the circumferential groove with SB, 24 protuberances are equally distributed on the end wall of RSP. The axial height h and the circumferential width of the protuberances are also the same as in the groove case; the both are $0.02D_t$. The RSP of $D' = 0.89D_c$ with SB is also examined. The number and the circumferential width of the protuberances are the same, while the axial height is changed from $0.02D_t$ to $0.04D_t$ and $0.06D_t$. Table 2 summarizes the suppression devices examined in the present numerical investigations.

Numerical Methods

A commercial software ANSYS CFX version 18.0 is used for CFD simulation. Steady simulation is conducted by solving Reynolds Averaged Navier-Stokes (RANS) equations with employing k-ω SST model for the turbulence closure. Figure 3 shows examples of enlarged meridional views around the inducer and the suppression devices of the computational models. In order to effectively conduct the simulation with moving reference frame, the stationary and rotating domains should be carefully chosen. The dark and light grey zones in the figure respectively show the stationary and rotating domains. The same mesh can be used for the rotating

domains in all the computational models. The interface between the rotating and stationary domains is treated by so-called frozen rotor interface where all flow variables are conserved across it with fixing the relative circumferential position between the connected domains. Figure 4 shows the entire flow domain in the case with no suppression device as an example. The inlet and outlet boundaries are located at $10D_t$ upstream and $6D_t$ downstream of the leading edge of inducer. The hub diameter is enlarged near the outlet boundary to avoid the occurrence of the backflow at the outlet boundary. As the boundary conditions, the mass flow rate is specified at the inlet boundary, while the constant static pressure at the outlet boundary. These may not be ideal boundary condition, since the total pressure is generally given upstream in the actual pump operation. Nevertheless, the present combination of boundary conditions would give the easier assessment of steep head breakdown point. On the solid walls, the non-slip wall condition is applied. The computational domain includes all passages of inducer in the case of the circumferential groove with swirl brake (SB), while only one passage is considered in the other cases and the rotational periodic boundary condition is applied.

In Table 2, the numbers of computational nodes used in the present simulations are summarized. The hexahedral meshes are created for all cases. Fifteen nodes are located radially in the tip clearance to well capture the tip leakage flow, since the resolution in this region is surely important to quantitatively well simulate the inlet backflow. The averaged non-dimensional wall distance of the first node on the blade surface is $y^+ \cong 0.7$, to well resolve the boundary layers on the blade surfaces. For discretization scheme, so-called high resolution scheme between the 2nd order central and the 1st order upwind differentiation schemes is employed for the advection terms in the discrete finite volume equations. In this scheme, a blending factor β (1 for the 2nd order central scheme and 0 for the 1st order upwind one) is introduced and the actual value of β is locally

determined on the basis of boundedness principles used by Barth and Jesperson [27]. For the diffusion terms, the spatial derivatives are calculated using the shape function which satisfies the Gaussian divergence theorem.

All numerical simulations are conducted with working fluid of water at room temperature. The rotational speed of inducer is set at $N = 5{,}000\text{min}^{-1}$. To evaluate the hydraulic performance of the inducer and the inlet backflow characteristics, the single-phase flow analysis is conducted. For the evaluation of suction performance of inducer, simulations considering cavitation are conducted. Zwart-Gerber-Belamri model [25] as a homogeneous cavitation model considering the dynamics of cavitation bubbles with a simplified Rayleigh-Plesset equation is employed, and the default values of the model constants given in ANSYS-CFX are used. The static pressure at the outlet boundary is decreased step-by-step to reduce the suction pressure, and at each pressure condition, i.e., NPSH (Net Positive Suction Head) condition, the hydraulic performance is evaluated. The suction performance is compared at three flow rates, $\phi_i = 0.086$ (high flow rate), $\phi_i = 0.061$ (near the best efficiency point of the model inducer) and $\phi_i = 0.012$ (extremely low flow rate), where ϕ_i is the flow coefficient defined as $\phi_i = Q/A_1 U_t$ with the volumetric flow rate of Q, the cross sectional area at the inlet of inducer, A_1 $(= \pi\,(D_c^2 - D_{h1}^2)/4\,, D_{h1}$: hub diameter at the inlet), and the tip velocity of inducer U_t $(= \pi D_t N/60)$.

The mesh independency check for the simulation of the model inducer has been conducted in our previous study [24]. We have used four different-size meshes, Fine (4,142,854 nodes), Medium (2,543,652 nodes), Coarse (1,030,904 nodes) and Very coarse (562,976) meshes. Even with the Very coarse mesh, we have obtained deviations from the Fine mesh case of less than 3% of the head, the shaft power, the efficiency and more importantly the flow rate of the inlet backflow at the flow coefficients of $\phi_i = 0.012$ and 0.061. Therefore, we have finally decided to use the

Coarse mesh to examine the effectiveness of the suppression devices proposed in this study. Since in cases with swirl brake (SB) the interaction between the rotating inducer blades and the stationary SB may have some impact on the hydraulic performances as well as on the inlet backflow, it is important to validate the present steady simulation. Therefore, an unsteady simulation has been conducted for the case with the reduced-diameter suction pipe ($D' = 0.78D_c$) with SB. The time step was chosen as 33.3×10^{-6}s which corresponds to the time duration for 1 degree rotation of inducer. Table 3 shows the comparison between the steady and unsteady simulations at the flow coefficients of $\phi_i = 0.012$ and 0.074. The head, the shaft power, the efficiency and the flow rate of inlet backflow just at the leading edge location of inducer obtained by the unsteady simulation are normalized by those of the steady simulation. It is seen that the difference between the results of unsteady and steady simulations is small enough, which has encouraged us to proceed with steady simulations throughout the present investigation.

Hydraulic Performance with Suppression Devices

Figure 5 shows the hydraulic performance of inducer with and without suppression devices of inlet backflow. The vertical axes in (a), (b) and (c) are head coefficient $\psi_i = 2(\bar{\bar{p}}_{t,out} - \bar{\bar{p}}_{t,in})/\rho U_t^2$, the power coefficient λ_i ($= T\omega/\rho A_1 U_t^3$) and the efficiency η_i ($= (\bar{\bar{p}}_{t,out} - \bar{\bar{p}}_{t,in})Q/T\omega = \psi_i\phi_i/2\lambda_i$), respectively. $\bar{\bar{p}}_{t,out}$ and $\bar{\bar{p}}_{t,out}$ are the mass-weighted averaged total pressure in the absolute frame evaluated at the inlet and outlet of the computational domain, and T is the total torque on the inducer and the shaft. The horizontal axis is the flow coefficient ϕ_i. By comparing the performance with the straight casing (Straight casing) and that with the circumferential groove (Groove) with swirl brake, the head is found to be almost the same. With the reduced-diameter suction pipe (RSP) without swirl brake, the head becomes smaller than

the straight casing in the inducer flow rate of $\phi_i < 0.086$. This tendency is more remarkable with the smaller inner diameter of suction pipe ($D'/D_c = 0.78$). By using the reduced-diameter suction pipe with swirl brake (RSP & SB), the head becomes larger than all other cases in $\phi_i < 0.086$. The shaft power is also larger with RSP & SB than in the other cases in this flow rate range, while the efficiency is larger. This seems to be due to the reduction of the pressure loss of the flow in the suction pipe through the suppression of the inlet backflow.

Inlet Backflow and Flow Recirculation

Figure 6 shows the inlet backflow rate ratio evaluated at $1D_t$ upstream from the leading edge of inducer plotted against the inducer flow coefficient ϕ_i. The flow rate of inlet backflow Q_{back} has been normalized by the working flow rate Q. In the case of the straight casing, the backflow starts to increase around $\phi_i = 0.086$ as ϕ_i decreases. By employing the circumferential groove with swirl brake (Groove), the inlet backflow is suppressed until $\phi_i = 0.049$, while, once the inlet backflow occurs, the flow rate significantly increases with the decrease of ϕ_i. No suppression effect of inlet backflow is observed in $\phi_i < 0.037$. By using the reduced-diameter suction pipe (RSP) without swirl brake, the inlet backflow is weakened in the whole flow rate range. The effect is more significant with RSP with the smaller inner diameter ($D'/D_c = 0.78$), while the suppression effect is still limited at very low flow rates of $\phi_i = 0.012$ and 0.024. Finally, by adding swirl brake onto the reduced-diameter suction pipe (RSP & SB), the suppression effect of inlet backflow can be enhanced. Especially, in the case of RSP ($D'/D_c = 0.78$) & SB ($h/D_t = 0.02$), the inlet backflow is completely removed. This fact indicates that the RSP combined with SB is very effective to suppress the inlet backflow provided that it is appropriately designed.

Figure 7 shows the meridional flow distributions of axial (upper figure) and circumferential (lower figure) components, (V_a and V_θ) of absolute flow velocity, at the lowest flow coefficient of $\phi_i = 0.012$. V_a and V_θ have been area-averaged and mass-weighted averaged respectively in the circumferential direction, and are normalized by the inducer tip velocity U_t. The flow direction is from left to right. First of all, in the case of straight casing (Fig. 7(a)), the inlet backflow extends far upstream as easily recognized by blue color region of V_a distribution. Inside the backflow, the circumferential velocity component V_θ is also large, that is a typical structure of inlet backflow forming the flow recirculation zone. In the case of circumferential groove with SB (Fig. 7(b)), the backflow goes over the groove clearly. The backflow region becomes thicker upstream of the groove, and the axial velocity of the main flow increases. In the cases of RSP without swirl brake (Figs. 7(c) and (e)), the backflow becomes thinner than the straight casing case (Fig. 7(a)), showing that RSP can suppress the inlet backflow to a certain degree, and the suppression effect is more significant with the smaller inner diameter RSP ($D'/D_c = 0.78$) . However, by adding the swirl brake (SB) with $h/D_t = 0.02$ onto RSP with $D'/D_c = 0.78$ (Fig. 7(f)), the backflow is completely removed. The backflow from inducer goes upstream along the casing wall and impinges on SB, loses the circumferential velocity completely at SB, and then merges into the main flow. As a result, almost no circumferential velocity exists at this cross-section, and therefore no radial pressure gradient forms, which seems to result in the complete prevention of the backflow from extending upstream. Then, no flow recirculation is observed. This suggests that the RSP with SB has a strong effect on suppressing the inlet backflow. In the case of RSP with $D'/D_c = 0.89$, although adding SB with $h/D_t = 0.02$ does not show the significant effect on the flow field (Fig. 7(d)), it has been separately confirmed that the inlet backflow could be completely removed by increasing the height of SB up to $h/D_t = 0.06$.

12

Inducer Suction Performance

Figure 8 shows the head drop curves of inducer with various suppression devices at three flow rates of (a) $\phi_i = 0.012$ (low flow rate), (b) 0.061 (near the best efficiency point) and (c) 0.086 (high flow rate). The vertical and horizontal axes are the head coefficient ψ_i and the normalized NPSH τ respectively. The normalized NPSH τ is defined as $\tau = 2(\bar{\bar{p}}_{t,in} - p_v)/\rho U_t^2$, where p_v is the vapor pressure of water. In addition to the RSPs of $D'/D_c = 0.79, 0.89$ and the RSP ($D'/D_c = 0.79$) with SB ($h/D_t = 0.02$), the RSP ($D'/D_c = 0.89$) with SB ($h/D_t = 0.06$) is examined since it was also found to be able to remove the inlet backflow completely.

At the low flow rate of $\phi_i = 0.012$ (Fig. 8(a)), with the decrease of τ, the head starts to decrease around $\tau = 0.025$ in the cases with the RSPs with SB (closed symbols). Despite that the head is larger, the suction performance with RSPs with SB is apparently better than that in the case with straight casing with which the head drop starts around $\tau = 0.1$. In the cases with RSP only, although the head is kept almost constant until $\tau = 0.05$, we could not stably continue the simulation with the further decrease of τ. Therefore, it seems that the RSPs with SB provides the better suction performance and the stable operation than the others. At the medium flow rate of $\phi_i = 0.061$ (Fig. 8(b)), the head drop curves with all suppression devices are comparable; the head starts to drop around $\tau = 0.05$ in all cases. Finally, at the high flow rate of $\phi_i = 0.086$ (Fig. 8(c)), the head gradually decreases with the decrease of τ in all cases, whereas the head starts to drop at lower NPSH ($\tau = 0.12$) with RSPs with SB than that in the other cases ($\tau = 0.15$). Therefore, it is shown that the suction performance with RSPs with SB is better also at the high flow rates.

As has been shown above, the employment of reduced-diameter suction pipe (RSP) with swirl brake (SB) at the inlet of inducer offers the possibilities of performance enhancement of

13

inducers such as the enhancement of efficiency, the preventions of the extension of the inlet backflow and the formation of flow-recirculation. It also offers the improvement of suction performance in the wide flow rate range. Although two different configurations of RSP with SB, $D'/D_c = 0.79$ with $h/D_t = 0.02$ and $D'/D_c = 0.89$ with $h/D_t = 0.06$, have been shown to be effective, we select the former one for the experimental validation after considering the structural strength. The method and the results will be provided in the next section.

EXPERIMENTAL EVALUATION

Experimental Method

Figure 9 shows a closed test loop used in this study. The tunnel is equipped with a cooling system of water as the working fluid, which enables us to conduct the experiment under a constant temperature. The pressure inside the tunnel can be adjusted by regulating the pressure inside the pressure tank by using a vacuum pump/ a compressor connected at the top of the tank. Figure 10 shows the schematic view of the test section where the test pump is installed. The test pump is a centrifugal pump having an inducer before the main impeller. The suction pipe and the casing around the inducer are made of transparent acrylic resin to enable the visual observation of cavitation in the inducer and in the suction pipe. Since no booster pump is installed in the test loop, the inducer cannot operate without the main impeller at high flow rates due to the low head of inducer against the flow resistance of the test loop. Therefore, we have determined to use the main impeller through this experimental investigation focusing on the effect of suppression devices. Before this investigation, we confirmed that the onset range of cavitation surge which occurs at the low flow rates are almost the same between the inducer with and without the main impeller in the case with no suppression device. We also checked the static pressure at the inducer outlet (③

in Fig. 10) at certain moderate flow rates, and it was confirmed that the pressure is not influenced by the main impeller at those flow rates.

Table 3 shows main specifications of the test pump. The main impeller is a semi-open type centrifugal one with 15 backward blades. The inducer is a three-bladed one with a tapered hub. It should be noted that, different from the model inducer used in the numerical investigation, this inducer has a sweptback leading edge. The test pump is the identical one used in our previous study [26], in which the suction performance and the occurrence of cavitation instabilities were fully investigated; we observed the cavitation surge with the low frequency and the large amplitude at low flow rates.

In this section, the effect of the suppression device developed through the above numerical investigation, namely the reduced-diameter suction pipe (RSP) with swirl brake (SB), on the onset range of cavitation surge as well as on the suction performance of the test pump is being experimentally investigated. To imitate RSP, a small-dimeter short pipe is inserted into the inducer casing with the inner diameter of D_c. The inner diameter of the short pipe is $D' = 0.784D_c$, and the cross-sectional area ratio of the pipe to the original casing is $A'/A_c = D'^2/D_c^2 = 0.615$. This situation with the smaller diameter pipe inserted is herein called "(only) RSP62", and the schematic view is shown in Fig. 11 (a). Next, the swirl brake (SB) is added to the short pipe. Instead of adding protuberances like those examined in our numerical simulation, the SB is machined by radially grooving the downstream end of the short pipe. The number of grooves is 24, and the width and the depth of them are $0.087D_t$ and $0.020D_t$, respectively. The added SB is geometrically resemble to that considered in our numerical study. The inner diameter and the cross sectional area are the same as in the case of RSP62. Therefore, we herein call this situation having the short pipe with SB "RSP62 with SB", and the schematic view is shown in Fig. 11 (b). The distance between the

downstream end of the short pipe with/without SB and the inducer leading edge is $l = 0.33D_t$, where D_t is the inducer tip diameter. This location is the closest one to the inducer without disturbing unsteady pressure measurements by using the pressure sensors which have been originally installed on the inducer casing wall.

All experiments are conducted under the constant rotational speed of the test pump, $N = 3000\text{min}^{-1}$. The flow rate of the pump Q is measured by electromagnetic flow meters installed downstream of the test section. As shown in Fig. 9, the discharge line from the test section is divided into two lines with the different inner diameter, and one of them is only used depending upon the flow rate condition. For the flow rate larger than 250L/min, the discharge line with the diameter of 50mm is used, and the flow rate Q is measured by an electromagnetic flow meter with the accuracy of 2.5L/min. On the other hand, for the smaller flow rate, the discharge line with the diameter of 20mm is used, and Q is measured by another electromagnetic flow meter within the possible maximum error of 1.5L/min. The pressure difference across the whole pump is measured by using a differential pressure transducer with the capacity of 1MPa and the improved accuracy of 1kPa connected to ① for the suction pressure and ④ for the discharge pressure as shown in Fig.

10. After considering the difference of dynamic pressures based on the area-averaged velocity between the discharge and the suction pressure measurement locations, the pump head H is evaluated. The shaft torque T is measured by a torque meter with the capacity of 100Nm and the accuracy of 0.5Nm. The torque meter is installed between the test pump and a driving motor. Then, the performance of the test pump is expressed by the flow coefficient ϕ, the head coefficient ψ, the shaft power coefficient λ and the efficiency η, and they are defined as follows;

$$\phi = \frac{Q}{A_2 U_2}, \qquad \psi = \frac{H}{U_2^2/2g}, \qquad \lambda = \frac{T\omega}{\rho A_2 U_2^3}, \qquad \eta = \frac{\rho g Q H}{T\omega} = \frac{\phi\psi}{2\lambda}$$

where A_2 is the passage area at the main impeller exit, U_2 the peripheral velocity of the main impeller, $\omega(= 2\pi N/60)$ the angular shaft speed, g the gravitational acceleration. In each performance evaluation, we use the time-averaged data in the duration of 20s (1000 shaft revolutions) with the sampling frequency of 1.5kHz, to enhance the statistical reliability. It should be noted that the measured torque T includes the mechanical loss torque which occupies the large portion of T. Therefore, we herein present the estimated uncertainties based on 95% confidence level only for ϕ and ψ, i.e., $\Delta\phi/\phi_{\text{bep}} = 0.008$ and $\Delta\psi/\psi_{\text{bep}} = 0.014$ in the most of cases, where ψ_{bep} is the head coefficient at the flow coefficient with the maximum efficiency, ϕ_{bep}.

For the evaluation of suction performance, the net positive suction head, NPSH, is calculated from the static pressure measured at the upstream pressure tap (① in Fig. 10) by a pressure transducer having the capacity of 200kPa abs. with the accuracy of 200Pa and the dynamic pressure based on the area-averaged axial velocity. Then, the normalized NPSH, τ, is defined as follows.

$$\tau = \frac{\text{NPSH}}{U_t^2/2g}, \qquad \text{NPSH} = \frac{p_{in} - p_v}{\rho g} + \frac{1}{2g}\frac{Q^2}{A_{in}^2}$$

where U_t is the inducer tip velocity, A_{in} is the cross-sectional area at the measurement point of upstream pressure, p_{in} is the measured absolute pressure and, p_v is the vapor pressure. The uncertainty of τ is estimated to be 0.004 typically in stable operation conditions, while it may increase in unstable conditions like those under the occurrence of strong cavitation surge.

The suction performance and the onset range of cavitation instabilities are investigated in detail with and without suppression devices. The working fluid is well degassed water, whose dissolved oxygen level is about 5-10% of saturation under the atmospheric condition. To evaluate the suction performance of the test pump, all above-mentioned measurements are conducted with

17

reducing the tunnel pressure stepwise by the vacuum pump, while keeping the flow rate and the rotational speed constant. The flow rate is adjusted by hand using the valve installed downstream of the test section. The upstream butterfly valve is fully opened. In order to detect the occurrence of cavitation instabilities, the pressure sensors are installed; two for $0.3D_t$ upstream of the inducer with 50 degrees different azimuthal locations, and another two for the volute casing as indicated by ② in Fig. 10. For upstream sensors, semiconductor-type transducers with the capacity of 200kPaG and the accuracy of 2kPa are used and installed via adapter filled with silicon oil to protect them from damage due to cavitation collapse without significant loosing of their frequency characteristics. For downstream sensors, small-size semiconductor-type transducers with the capacity of 2MPaG and the accuracy of 30kPa are flush-mounted on the volute casing wall. The sampling frequency of the measurement is 5000 Hz. For the confirmation of the occurrence of cavitation instabilities, a visual observation of cavitation in the inducer section is also conducted through the acrylic casing by using a high-speed camera with the frame rate of 2000 frame/s.

Hydraulic performances with suppression devices

Figure 12 shows the hydraulic performance curves of the test pump with the reduced-diameter suction pipe (RSP62), RSP62 with Swirl brake (SB), and without RSP (Straight casing) in the non-cavitating condition. The flow coefficient ϕ, head coefficient ψ, the power coefficient λ and the efficiency η have been normalized by those at the best efficiency point (subscript of bep) with the straight casing. Looking at the head coefficient, it is seen that the head coefficient is almost the same in the flow rate larger than the best efficiency point ($\phi/\phi_{\text{bep}} \geq 1$). On the other hand, if the flow rate is decreased than that at the best efficiency point, the difference of the head

becomes significant among the three cases. As shown later, the static pressure at the suction measurement point is increased at low flow rates with the decrease of the flow rate, which seems to be due to the growth of the inlet backflow from inducer. This increase of the suction pressure is more apparent in the case with the straight casing. As a result, the head coefficient is smaller in the case of "Straight casing" than in the cases of both "RSP62" and "RSP62 with SB". Actually, it was confirmed in our previous study [28] that the head estimated using the tank pressure with considering the head loss of suction pipe instead of the measured suction pressure was almost the same in the cases with the straight casing and with only RSP62. Also, the estimated head was larger in RSP62 with SB, implying the possibility of the improvement of hydraulic performance of the test pump at low flow rates by using RSP62 with SB. The efficiency in the case with only RSP62 looks better than the others at high flow rates, but it should be noted that small deviation of the mechanical loss could affect the efficiency; we will not go into the detail.

Suppression of inlet backflow with suppression devices

In our numerical investigations, it was found that the reduced-diameter suction pipe (RSP) with swirl brake (SB) has a remarkable effect on preventing the inlet backflow from extending upstream. Since the measurement of the inlet backflow is not very easy, the backflow is investigated by referring to the behavior of the suction pressure of the pump. The static pressure upstream of inducer is expected to begin to increase when the inlet backflow reaches the measurement position. We estimate the increment of static pressure Δp_{in} due to the inlet backflow using the following equation.

$$\Delta p_{in} = p_{in} - \left[p_{tank} - \frac{1}{2}\rho(1 + \zeta)\left(\frac{Q}{A_{in}}\right)^2 \right]$$

where p_{in} is the measured suction pressure (at ① in Fig. 10), and the bracket in the right-hand

side is the suction pressure at the same location expected if there is no influence of the inlet

backflow. The latter is estimated from the tank pressure p_{tank} by using Bernoulli's equation with

considering the head loss of the suction pipe with the pre-measured loss coefficient of ζ. Figure

13 shows the normalized pressure increment of $2\,\Delta p_{in}/\rho U_t^2$ against the flow coefficient ratio

ϕ/ϕ_{bep}. It can be seen that, in the case with the straight casing, the suction pressure begins to

increase at ϕ/ϕ_{bep}=0.88 with the decrease of the flow rate, and the increase is accelerated below

ϕ/ϕ_{bep}=0.57. By applying only RSP62, the increment of the suction pressure becomes smaller,

which indicates that the inlet backflow is well suppressed. However, the suppression effect is

limited, and it seems that the inlet backflow reaches the measurement position when the flow rate

is ϕ/ϕ_{bep}=0.42. Finally, by applying RSP62 with SB, the increment of suction pressure is almost

diminished, and the small increment is observed only at the shut-off condition (ϕ/ϕ_{bep}=0). From

this experimental observation, it can be said that RSP especially with SB is very effective to

prevent the inlet backflow of the pump from extending upstream.

Suction performance with suppression devices

Figure 14 compares the head drop curves of the test pump against the decrease of NPSH

in the cases with the straight casing, RSP62, and RSP62 with SB at (a) a very low flow rate

(ϕ/ϕ_{bep}=0.036), (b) the best efficiency point (ϕ/ϕ_{bep}=1.0) and (c) a very high flow rate

(ϕ/ϕ_{bep}=1.43).

At the low flow rate (Fig. 14(a)), the head drop curve is clearly improved by applying RSP62 and RSP62 with SB, and the improvement is more in RSP62 with SB; in RSP62, the head drop starts to occur at the normalized NPSH of $\tau=0.04$, while it does at $\tau=0.03$ in RSP62 with SB. This tendency agrees with our numerical investigation shown in Fig. 8(a), suggesting again that the suction performance can be well enhanced by applying RSP62 with SB at low flow rates.

At the maximum efficiency point (Fig. 14(b)), the head drop curves are basically the same in all cases; once the head drop starts, the head sharply drops. It seems to drop slightly earlier in RSP62 with SB, but the difference from the other cases is almost negligible.

At the high flow rate (Fig. 14 (c)), the suction performance is clearly deteriorated when either RSP62 or RSP62 with SB is used. The head drop curves are almost the same in RSP62 and RSP62 with SB. At high flow rates, the incidence angle of the flow against the inducer blade is small, and it is actually close to zero at the flow rate of $\phi/\phi_{\mathrm{bep}}=1.43$. Because of the small inner diameter of RSP62, the axial velocity is larger (60% larger than that in the original straight casing) at the connection location of RSP62. Although it diffuses downstream, the diffusion seems to be insufficient at the inlet of inducer at high flow rates, which possibly makes the incidence angle negative. Actually, we observed the occurrence of cavitation from the leading edge on the pressure side. This suggests that the earlier head drop in RSP62 and RSP62 with SB is caused by the cavitation on the pressure side at this high flow rate. This negative feature of RSP and RSP with SB may be relieved by optimizing their distance from the inducer.

Suppression of cavitation surge with suppression devices

As presented above, the reduced-diameter suction pipe with swirl brake (RSP with SB) is effective to improve the suction performance at the low flow rates as well as to suppress the

extension of inlet backflow region. However, the further investigation on cavitation instabilities especially on cavitation surge is necessary to ensure the operation reliability of the pump. Here, we report the onset map of cavitation surge based on the results of unsteady pressure measurements and high speed observations.

Figure 15 shows typical examples of FFT analyses of pressure fluctuations at the low flow rate of ϕ/ϕ_{bep}=0.29, that is a typical condition where the cavitation surge possibly occurs, in the cases with (a) the straight casing, (b) RSP62 and (c) RSP62 with SB. The top and middle figures show the contour maps of pressure fluctuation amplitudes measured upstream of inducer and on the volute casing wall, respectively. The bottom figure shows the head drop curve. In the top and middle figures, the vertical axis is the normalized frequency f/f_n (f_n: shaft speed frequency), while the horizontal axis is the normalized NPSH τ. The color contour map is drawn by $|\Delta\psi_s|$, the amplitude of pressure fluctuation normalized by $\rho U_2^2/2$. When a fluctuation component at a certain frequency is detected, we also check the cross-correlation of this component at the same streamwise location (upstream or downstream) with different azimuth angles. If the phase angle is zero, the fluctuation is regarded as to be caused by axial (surge-like) instabilities like cavitation surge. If the phase angle is a multiple of azimuth angle difference of two measurement locations, the fluctuation is regarded as to be caused by rotating instabilities like rotating cavitation. The type of instabilities responsible for the observed pressure fluctuation is identified by this way. We also check the occurrence of instabilities from the visual observation of cavitation behavior.

As NPSH is decreased, a distinct frequency component around f/f_n=0.2~0.25 firstly appears only in the case with straight casing (Fig. 15(a)). This is observed only in the upstream pressure fluctuation. From the phase analysis and the visual observation, it has been found that this component is caused by the backflow vortex whirling in the suction pipe, which is known to

originate from the instability of shear layer between incoming main flow and the swirling backflow. In the cases of RSP62 (Fig. 15(b)) and RSP62 with SB (Fig. 15(c)), this component is not at all observed, implying that the inlet backflow is well suppressed by these devices at this flow rate.

With the further decrease of NPSH, the large amplitude of pressure fluctuation is observed in the upstream pressure fluctuation as indicated by (i). From the visual observation, it has been found to be caused by the cavitation surge. In the case with the straight casing, the fluctuation looks to be wide-banded, but it is actually composed of the surge frequency component and its harmonics. A weak component corresponding to the cavitation surge can be confirmed also in the downstream pressure fluctuation. The amplitudes of the surge component and its harmonics increase with the decrease of NPSH, and, the head coefficient, which is evaluated from the time-averaged head, drops gradually during the growth of cavitation surge. By applying only RSP62, the onset range of cavitation surge is significantly narrowed as can be clearly seen in Fig. 15(b). Even when the cavitation surge occurs, the amplitude of pressure fluctuation becomes quite smaller than that with the straight casing. Therefore, it is shown that applying RSP offers the suppression of cavitation surge to a certain degree. When the RSP62 with SB is applied, the pressure fluctuations due to the cavitation surge are not at all observed, as shown in Fig. 15(c), showing the excellent suppression effect of RSP62 with SB on cavitation surge. Instead, the surge mode oscillation with the normalized frequency of $f/f_n \cong 0.05$ appears during the steep head drop as indicated by (ii) in the figure. The amplitude of pressure fluctuation is small, and the flow rate fluctuation was not detected by an electromagnetic flow meter installed on the suction pipe. Since this component was observed only at this condition with steep head drop, this phenomenon is thought to be the choked surge [29].

Figure 16 shows the onset map of cavitation surge plotted in the normalized NPSH τ and the flow rate ratio ϕ/ϕ_{bep} plane in the cases with (a) the straight casing, (b) RSP62 and (c) RSP62 with SB. The plots in the figure indicate the examined operating conditions of τ and ϕ/ϕ_{bep}, and the cavitation surge is observed in the conditions with closed symbols. In the figures, the solid and broken lines show the 3% and 50% head drop NPSH, respectively. In the case with the straight casing, the cavitation surge occurs in the wide flow rate range. The cavitation surge starts to occur at the larger NPSH than that with 3% head drop, suggesting that the head drop gradually progresses with the growth of cavitation surge. By applying RSP62, the onset range of cavitation surge is significantly narrowed, but the suppression effect is limited; at the flow rate ratios ϕ/ϕ_{bep} less than 0.3, the cavitation surge still occurs in the wide range of NPSH. In this flow rate range, the suppression of the inlet backflow is insufficient as can be seen in Fig. 13. This suggests that the suppression of the inlet backflow is essential for the suppression of cavitation surge. On the other hand, by applying RSP62 with SB, the cavitation surge is not at all observed, showing the excellent suppression effect on the cavitation surge. The doubled circle symbols indicate the onset of chocked cavitation which is observed only during the drastic head drop in the limited flow rate range of ϕ/ϕ_{bep}<0.5. Considering that the pumps will not be operated after the head drop, it is plausible that the operation reliability of the pump could be well enhanced by using RSP62 with SB.

CONCLUSIONS

In the present study, in order to suppress the inlet backflow and the cavitation surge which often occur in the low flow rate operation of turbopump with inducer, the reduced-diameter suction pipe (RSP), whose diameter is smaller than the inducer casing, equipped with swirl brake (SB) at

is end was proposed. The effectiveness of this new device was validated through the numerical simulation with CFD and experiment.

In the numerical validation, several geometries of RSP with SB were examined by CFD. The results were compared with the normal straight casing, with the circumferential groove with SB, and with only RSP. In the case of RSP, two different inner diameters were examined. As a result, it was found that, by applying RSP of smaller inner diameter with SB, the extension of inlet backflow was almost perfectly suppressed through removing the circumferential velocity in the backflow from inducer by SB. In the case with RSP of larger inner diameter, the suppression effect was insufficient, but it was separately confirmed that the inlet backflow was suppressed by the increment of the axial height of SB. Therefore, it was thought that SB with the sufficient axial height or radial length could well suppress the inlet backflow. In addition, the predicted hydraulic performance and suction performance showed no deterioration by RSP with SB but the possibility of enhancement at low flow rates.

One of the proposed RSP with SB, that is RSP of the smaller inner diameter with SB, was manufactured, and the experimental evaluation of the effectiveness of this device was conducted. The RSP and the RSP with SB were imitated by inserting a short pipe without/with SB machined at its end into the original casing. The experimental results were compared with those with the normal straight casing. From the behavior of measured suction pressure against the working flow rate, it was suggested that the extension of the inlet backflow was significantly suppressed by RSP with SB; only at the shut-off condition, the backflow seemed to goes over the SB section and to reach the pressure measurement location. Therefore, it seemed that RSP with SB could well prevent the extension of inlet backflow. Only RSP also could prevent the extension of inlet backflow to a certain degree; the effect is insufficient at very low flow rates.

The suction performance of the test pump was compared among three cases of straight casing, only RSP, and RSP with SB. At the low flow rate, the suction performance was well improved by RSP with SB. The RSP also gave the improvement of the performance, which was less than the RSP with SB. This seemed to be in a close relation with the occurrence of cavitation surge; the large amplitude of cavitation surge could lead to the decrease of the time averaged head, which could cause the earlier deterioration of head with the growth of cavitation surge. At the maximum efficiency flow rate, the suction performance was almost the same in the examined three cases while slightly worse in RSP with SB. Finally, at the very high flow rate, the suction performances in the cases of both RSP and RSP with SB were worse than that in the straight casing. This seemed to be due to the excessive axial flow velocity due to the small inner diameter in the both RSP and RSP with SB; the incidence angle of the flow against the inducer blade could be negative, which might easily lead to the head drop with the development of cavitation on the pressure side of the inducer blade. This negative effect of RSP and RSP with SB may be relieved by optimizing their distance from the inducer.

In the test pump with the normal straight casing, the cavitation surge was observed in the flow rate less than the best efficiency point. By applying only RSP, the cavitation surge was significantly suppressed, and even when the cavitation surge occurred, the amplitude of pressure fluctuation became quite smaller. Therefore, it will be certain that applying RSP offers the suppression of cavitation surge to a certain degree. When the RSP62 with SB was applied, the cavitation surge was completely suppressed even at extremely low flow rates. Although a weak one-dimensional instability which seemed to be choked surge was observed during the final head drop at low NPSH, it can be concluded that RSP with SB offers the significant enhancement of the operation reliability of the pump.

ACKNOWLEDGMENT

NOMENCLATURE

A_1 Flow passage area at inlet of inducer   [m²]

A_2 Passage area at main impeller exit [m²]

A_{in} Cross-sectional area at suction pressure measurement point [m²]

c Tip clearance [m]

D' Inner diameter of reduced-diameter suction pipe (RSP) [m]

D_c Inner diameter of inducer casing [m]

D_{h1}, D_{h2} hub diameters of inducer at inlet and outlet [m]

D_t Tip diameter of inducer [m]

f Frequency [Hz]

f_N Shaft speed frequency [Hz]

g Gravity acceleration [m/s²]

H Head [m]

N Shaft rotational speed [min⁻¹]

NPSH   Net positive suction head [m]

p Static pressure [Pa]

p_{loss} Estimated loss pressure of suction pipeline {pa}

p_{in} Static pressure at inlet of inducer [Pa]

$p_{t,in}$ Total pressure at inlet of inducer [Pa]

p_v Vapor pressure [Pa]

Q Flow rate [m³/s]

Q_{back} Calculated flow rate of inlet backflow [m³/s]

T Shaft torque [Nm]

U_2 Impeller outlet rotational velocity [m/s]

U_t Inducer tip velocity [m/s]

V_a, V_θ Axial and circumferential components of flow absolute velocity [m/s]

Z_i, Z_m Number of blades of inducer and main impeller

Δp_{in} Estimated increase of static pressure by inlet backflow [Pa]

η, η_i Efficiencies of test pump and model inducer

λ, λ_i Power coefficients of test pump and model inducer

ρ Density of water [kg/m³]

τ Normalized NPSH ($= 2g\mathrm{NPSH}/U_t^2$)

ϕ, ϕ_i Flow coefficients of test pump and model inducer

ψ, ψ_i Head coefficients of test pump and model inducer

REFERENCES

[1] Jacobsen, J. K., 1971, "Liquid Rocket Engine Turbopump Inducers", NASA-SP-8052.

[2] Acosta, A. J., 1958, "An Experimental Study of Cavitating Inducer", Proc. the 2nd Symposium of Naval Hydrodynamics, pp. 537-557.

[3] Kamijo, K., Shimura, T. and Watanebe, T., 1977, "An Experimental Investigation of Cavitating Inducer Instability," ASME Paper 77-Wa/FE-14, pp. 1-9.

[4] Tsujimoto, Y., Yoshida, Y., Maekawa, Y., Watanabe, S. and Hashimoto, T., 1997, "Observations of Oscillating Cavitation of an Inducer," ASME J. Fluids Eng., **119**(4), pp. 775-781. DOI: 10.1115/1.2819497

[5] Pace, G., Valetini, D., Pasini, A., Torre, L., Fu, Y. and d'Agostino, L., 2015, "Geometry Effects on Flow Instabilities of Different Three-Bladed Inducers," ASME J. Fluids Eng., **137**(4), 041304. DOI: 10.1115/1.4029113

[6] Brennen, C. E. and Acosta, A. J., 1976, "The Dynamic Transfer Function for a Cavitating Inducer," ASME J. Fluids Eng., **98**(2), pp. 182-191. DOI: 10.1115/1.3448255

[7] Tsujimoto, Y., Kamijo, K. and Yoshida, Y., 1993, "A Theoretical Analysis of Rotating Cavitation in Inducers," ASME J. Fluids Eng., **115**(1), pp. 135-141. DOI: 10.1115/1.2910095

[8] Tsujimoto Y., Kamijo, K. and Brennen, C. E., 2001, "Unified Treatment of Flow Instabilities of Turbomachines," AIAA J. Prop. and Power, **17**(3), pp. 636-643. DOI: 10.2514/2.5790

[9] Watanabe, S. and Tsujimoto, Y., 2021, "Prediction of Cavitation Surge Onset Point by One-Dimensional Stability Analysis," Int. J. Fluid Machinery and Systems, **14**(2), pp. 207. DOI: 10.5293/IJFMS.2021.14.2.199

[10] Watanabe, S., Sato, K., Tsujimoto, Y. and Kamijo, K., 1999, "Analysis of Rotating Cavitation in a Finite Pitch Cascade Using a Closed Cavity Model and a Singularity Method," ASME J. Fluids Eng., **121**(4), pp. 135-141. DOI: 10.1115/1.2823544

[11] Watanabe, S., Tsujimoto, Y., Franc, J. P. and Michel, J. M., 1998, "Linear Analysis of Cavitation Instabilities," Proc. 3rd International Symposium on Cavitation, Grenoble, France, **I**, pp. 347–352

[12] Kang, D., Watanabe, T., Yonezawa, K., Horiguchi, H., Kawata,Y., and Tsujimoto, Y., 2009, "Inducer Design to Avoid Cavitation Instabilities," Int. J. Fluid Machinery and Systems, **2**(4), pp. 439-448. DOI: 10.5293/IJFMS.2009.2.4.439

[13] Kamijo, K., Yoshida, M. and Tsujimoto, Y., 1993, "Hydraulic and Mechanical Performance of LE-7 LOX Pump Inducer," AIAA J. Prop. and Power, **9**(6), pp. 819-826. DOI: 10.2514/3.23695

[14] Shimiya, Y., Fujii, A., Horiguchi, H., Uchiumi, M., Kurokawa, J. and Tsujimoto, Y., 2008, "Suppression of Cavitation Instabilities in an Inducer by J-Groove," ASME J. Fluids Eng., **130**(2), 021302. DOI: 10.1115/1.2829582

[15] Kang, D., Arimoto, Y., Yonezawa, K., Horiguchi, H., Kawata, Y., Hah, C. and Tsujimoto, Y., 2010, "Suppression of Cavitation Instabilities in an Inducer by Circumferential Groove and Explanation of Higher Frequency Components," Int. J. Fluid Machinery and Systems, **3**(2), pp. 137-149. DOI: 10.5293/IJFMS.2010.3.2.137

[16] Tomaru, H., Ugajin, H., Kawasaki, S. and Nakano, M., 2007, "Suppression of Cavitation Surge in a Turbopump Inducer by the Backflow Restriction Step," Proc. the 43rd AIAA/ASME/SAE/ASEE Joint Propulsion Conference, Cincinnati, Ohio, AIAA-2007-5538.

[17] Watanabe, S., Inoue, N., Ishizaka, K., Furukawa, A. and Kim, J.-H., 2010, "Internal Flow of a Two-Bladed Helical Inducer at an Extremely Low Flow Rate," Int. J. Fluid Machinery and Systems, **3**(2), pp. 129-136. DOI: 10.5293/IJFMS.2010.3.2.129

[18] Furukawa, A., Ishizaka, K. and Watanabe, S., 2002, "Flow Measurement in Helical Inducer and Estimate of Fluctuating Blade Force in Cavitation Surge Phenomena," JSME Int. J. Series B Fluids and Thermal Engineering, **45**(3), pp. 672-677. DOI: 10.1299/jsmeb.45.672

[19] Sloteman, D. P., Cooper, P., and Dussourd, J. L., 1984, "Control of Backflow at the Inlets of Centrifugal Pumps and Inducers," First International Pump Symposium, Houston, TX, pp. 9–22.

[20] Lundgreen, R., Maynes, D., Gorrell, S. and Oliphant, K, 2019, "Increasing Inducer Stability and Suction Performance With a Stability Control Device," ASME J. Fluids Eng., **141**(1), 011204. DOI: 10.1115/1.4040098

[21] Kim, J.-H., Ishizaka, K., Ishizaki, M., Watanabe, S. and Furukawa, A., 2008, "Suppression Effect of Upstream Installed Ring-Shaped-Obstacle Plate on Cavitation Surge in Pump Inducers," J. Fluid Science and Technology, **3**(1), pp. 1-10. DOI: 10.1299/jfst.3.1

[22] Tanaka, Y., Shirakigawa K., Watanabe, S. and Tsuda, S., 2017, "Cavitation Performance of Helical Inducer with Reduced-Diameter Suction Conduit," Proc. the Ninth JSME-KSME Thermal and Fluids Engineering Conference (TFEC9), Naha, Japan, TFEC9-1388.

[23] Tsubouchi, K., Sakaguchi, M., Toyoshima, M., Horiguchi, H. and Sugiyama, K., 2015, "Suppression of Cavitation Instabilities in an Inducer by Circumferential Groove with Swirl Brake," Proc. the 13th Asian International Conference on Fluid Machinery (AICFM13), Tokyo, Japan, AICFM13-120.

[24] Tanaka, Y., Kitabata, T., Nasu, K., Watanabe, S., Ohashi, S., Sakata, A. and Matsunaga, Y., 2021, "Evaluation of Suction Performance of Inducer with Splitter Blade," Int. J. Fluid Machinery and Systems, **14**(1), pp. 13-24. DOI: 10.5293/IJFMS.2021.14.1.13

[25] Zwart, P. J., Gerber, A. G. and Belamri, T., 2004, "A Two-Phase Flow Model for Predicting Cavitation Dynamics," Proc. Fifth Int. Conf. on Multiphase Flow, Yokohama, Japan, Paper No. 152.

[26] Morii, T., Tanaka, Y., Watanabe, S., Ohashi, S. and Matsunaga, Y., 2019, "Suction Performance and Cavitation Instabilities of Turbopumps with Three Different Inducer Design," Int. J. Fluid Machinery and Systems, **12**(2), pp. 128-135. DOI: 10.5293/IJFMS.2019.12.2.128

[27] Barth, T.J. and Jesperson, D.C, 1989, "The Design and Application of Upwind Schemes on Unstructured Meshes," Proc. AIAA 27th Aerospace Sciences Meeting, Reno, NV, AIAA 1989-366. DOI: 10.2514/6.1989-366

[28] Tanaka, Y., Morii, T., Watanabe, S., Ohashi, S., Sakata, A. and Matsunaga, Y., 2020, "Suppression Effect of Reduced-Diameter Suction Pipe on Cavitation Surge in a Turbopump with Inducer," (in Japanese), Turbomachinery, **48**(10), pp. 577-586. DOI: 10.11458/tsj.48.10_577

[29] Watanabe, T., Kang, D., Cervone, A., Kawata, Y. and Tsujimoto, Y., 2008, "Choked Surge in a Cavitating Turbopump Inducer," Int. J. Fluid Machinery and Systems, **1**(1), pp. 64-75. DOI: 10.5293/IJFMS.2008.1.1.064

Figure Captions List

Fig. 9   Closed test loop

Fig. 10   Schematic view of test section. Straight casing case is shown as an example

Fig. 11   Installation of suppression device
                 (a) RSP62 only
                 (b) RSP62 with SB

Fig. 12   Hydraulic performance with/without suppression device

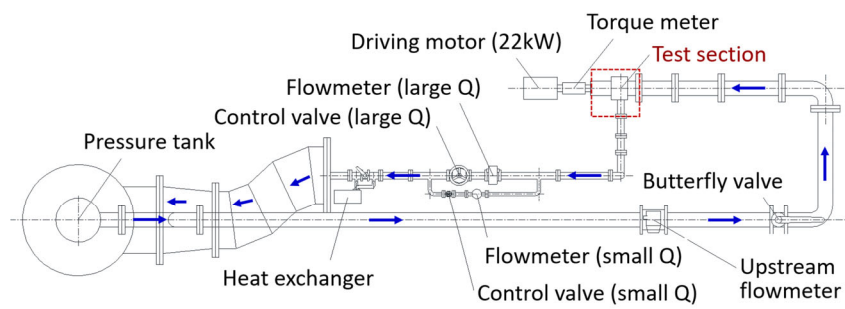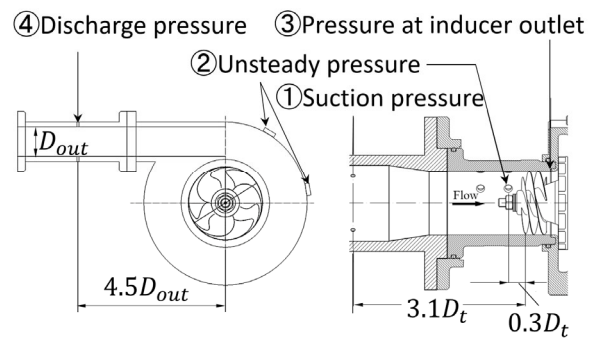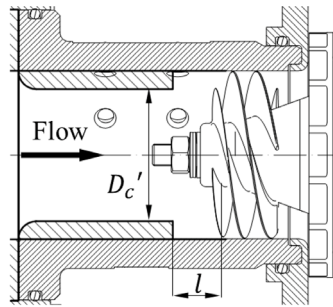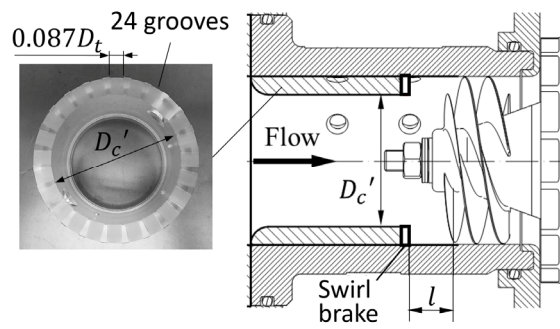Fig. 13   Increase of static pressure at inlet of test section by inlet backflow

Fig. 14   Suction performance curves at three different flow rates
                 (a) ϕ/ϕ_{bep}=0.036
                 (b) ϕ/ϕ_{bep}=1.0
                 (c) ϕ/ϕ_{bep}=1.43

Fig. 15   Typical examples of FFT analyses of upstream (top) and downstream (middle) pressure fluctuations along with head breakdown curve (bottom). Normalized flow rate is ϕ/ϕ_{bep}=0.29. (i) denotes onset range of cavitation surge, while (ii) denotes choked surge which occurs during head degradation.
                 (a) Straight casing
                 (b) RSP62 only
                 (c) RSP62 with SB

Fig. 16   Onset region of cavitation surge with/without suppression device
                 (a) Straight casing
                 (b) RSP62 only
                 (c) RSP62 with SB

Table Caption List

Fig. 1 Schematic view of model inducer

(a) Groove with swirl brake (SB)

(b) Reduced-diameter suction pipe (RSP)

(c) Reduced-diameter suction pipe (RSP) combined with swirl brake (SB)

Fig. 2 Inlet geometries with suppression device
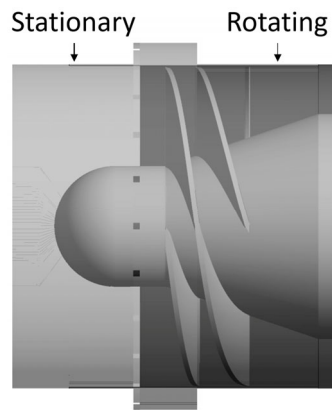
(a) Groove with swirl brake (SB)
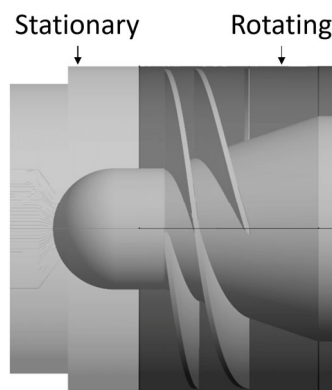
(b) Reduced-diameter suction pipe (RSP)
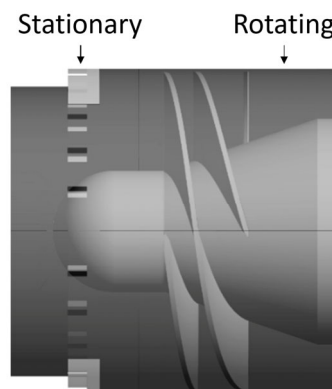
(c) RSP with SB

Fig. 3 Rotating and stationary flow domains in numerical model

Fig. 4 Computational domain (no suppression device)
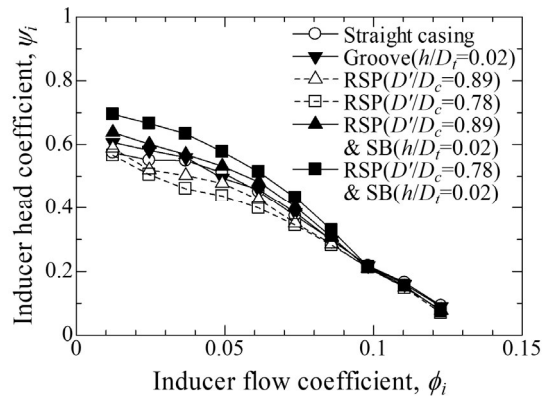
(a) Head coefficient
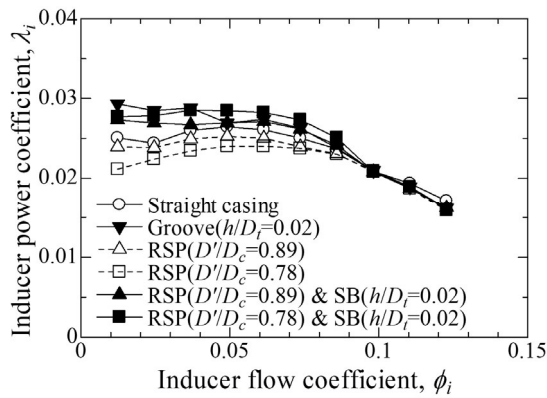
(b) Power coefficient
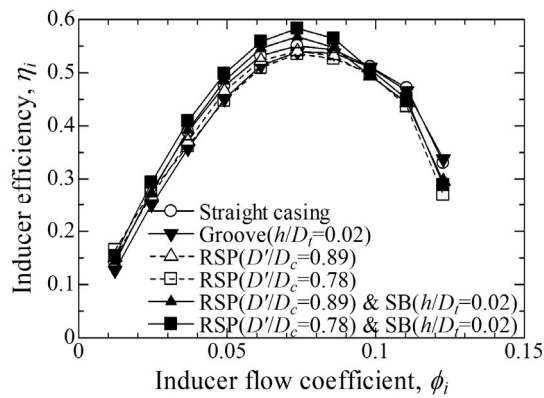
(c) Efficiency

Fig. 5 Hydraulic performance curves obtained by numerical simulation
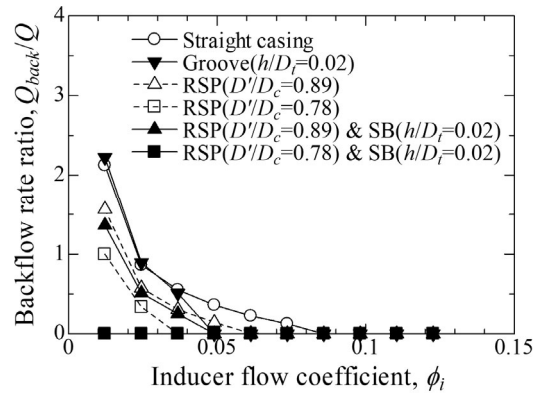
Fig. 6 Backflow rate ratio evaluated at $1D_t$ upstream of leading edge of inducer
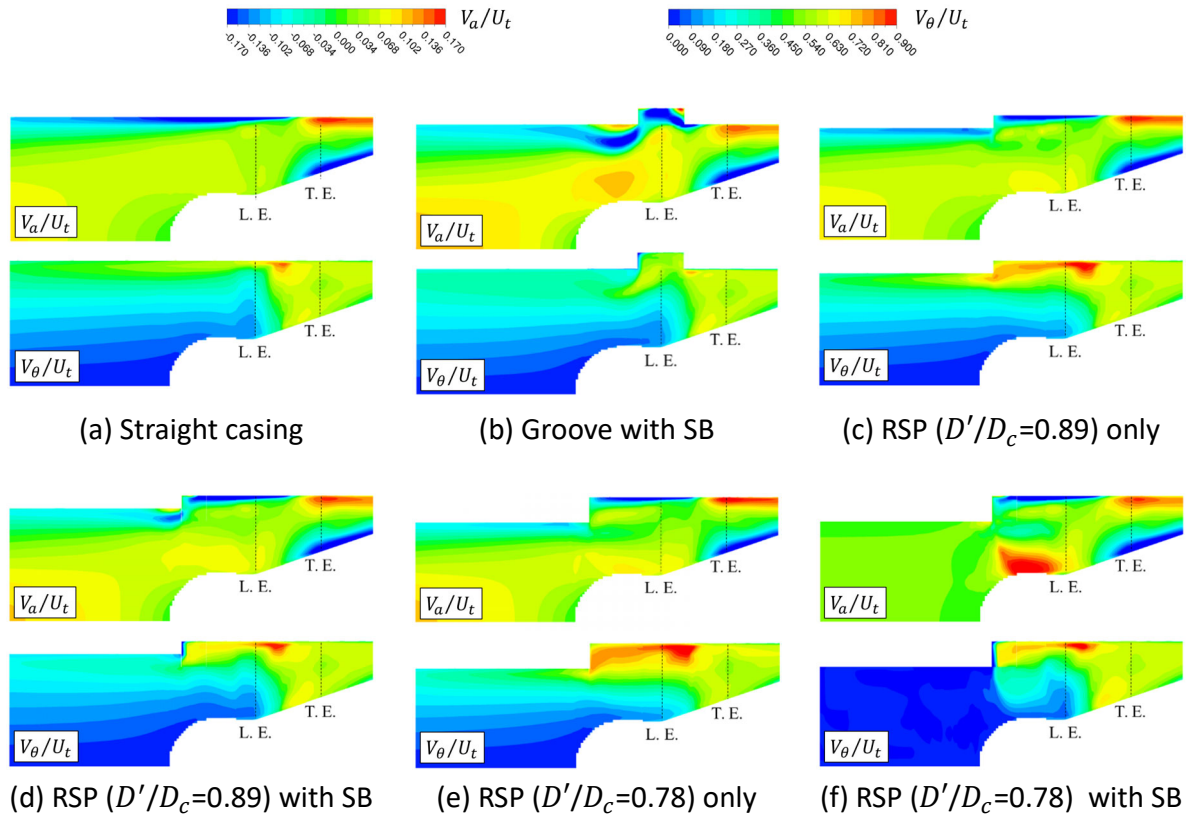
Fig. 7 Velocity distribution at ϕ_i=0.012 (Upper: Axial velocity V_a/U_t, Lower: Circumferential velocity V_θ/U_t)

(a) ϕ_i=0.012

(b) ϕ_i=0.061
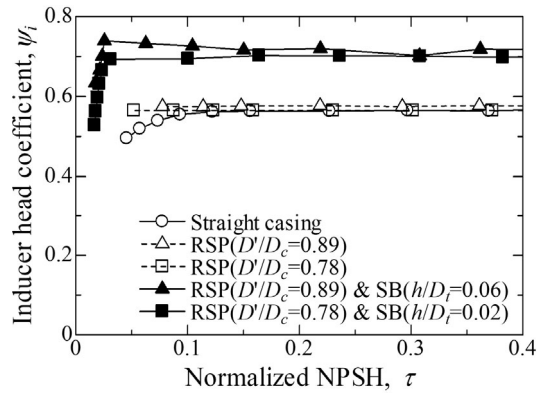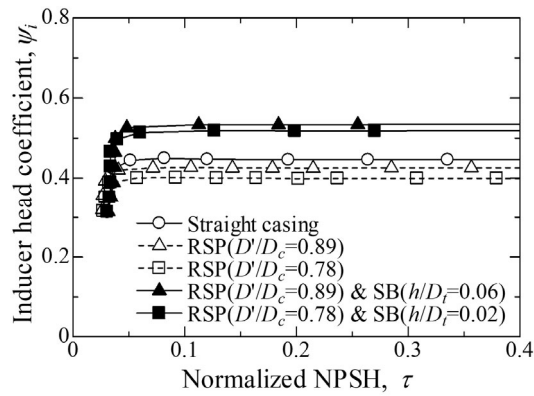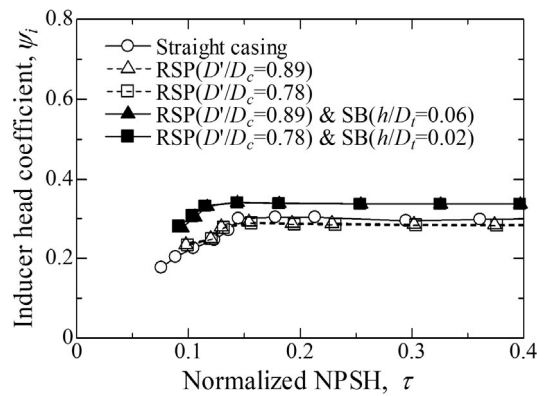
(c) ϕ_i=0.086

Fig. 8 Head breakdown curves obtained by numerical simulation

Fig. 9 Closed test loop

Fig. 10 Schematic view of test section. Straight casing case is shown as an example

(a) RSP62 only

(b) RSP62 with SB
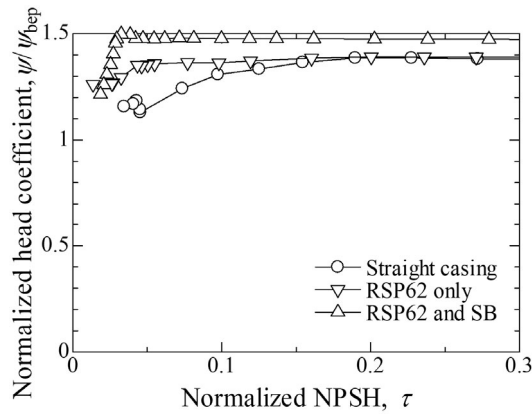Fig. 11 Installation of suppression device
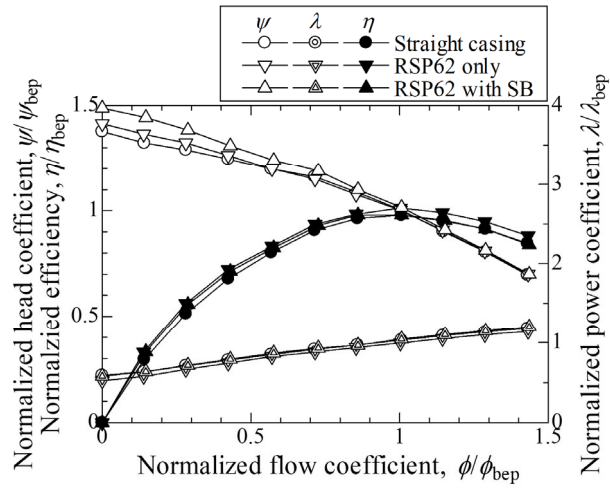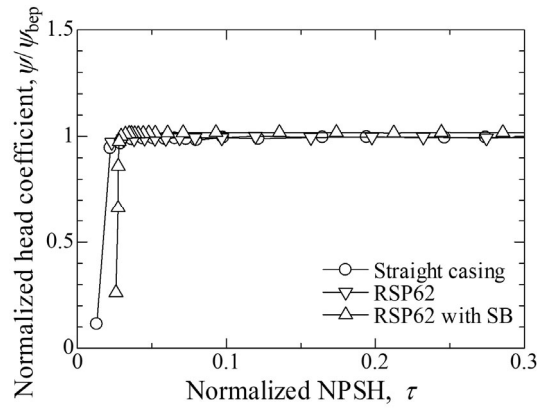
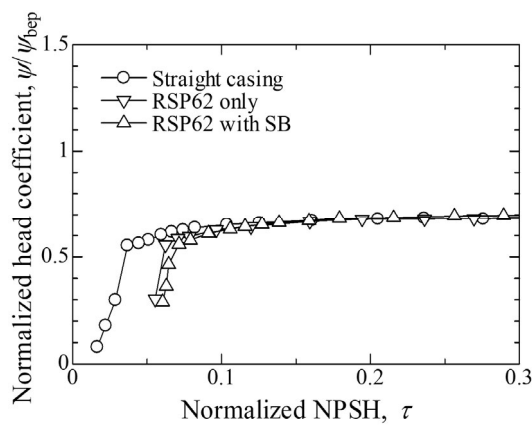Fig. 12 Hydraulic performance with/without suppression device
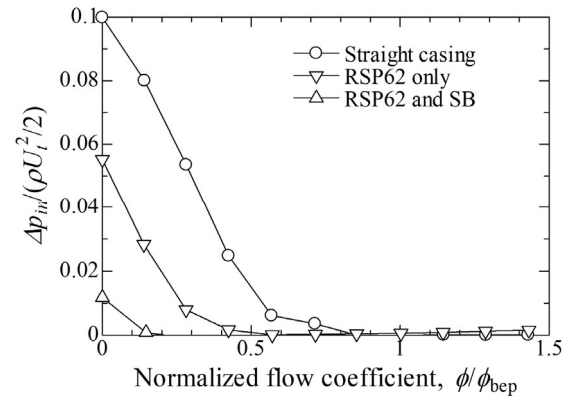
Fig. 13 Increase of static pressure at inlet of test section by inlet backflow

(a) ϕ/ϕ_{bep}=0.036

(b) ϕ/ϕ_{bep}=1.0

(c) ϕ/ϕ_{bep}=1.43
Fig. 14 Suction performance curves at three different flow rates

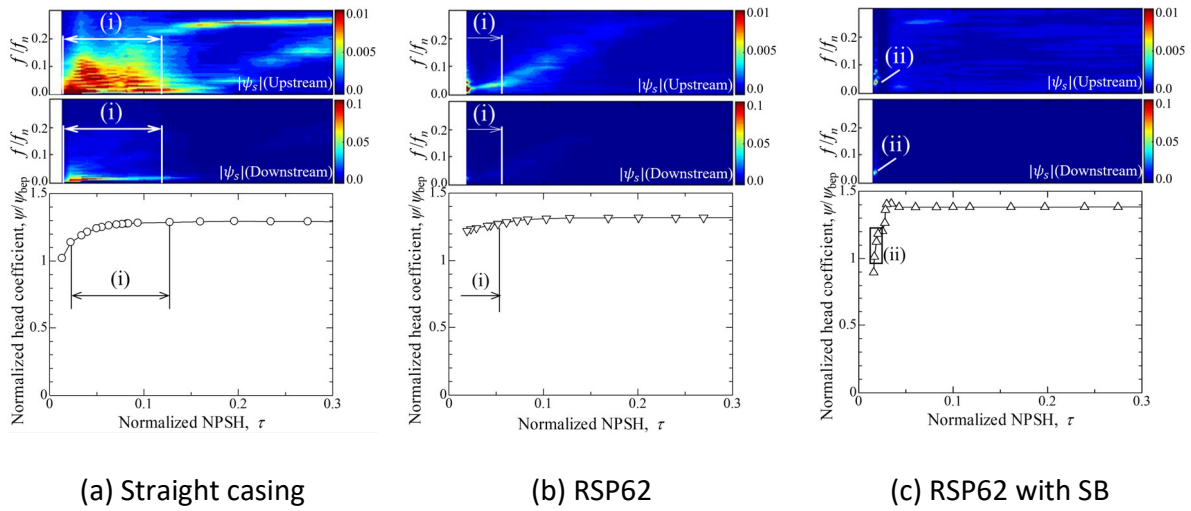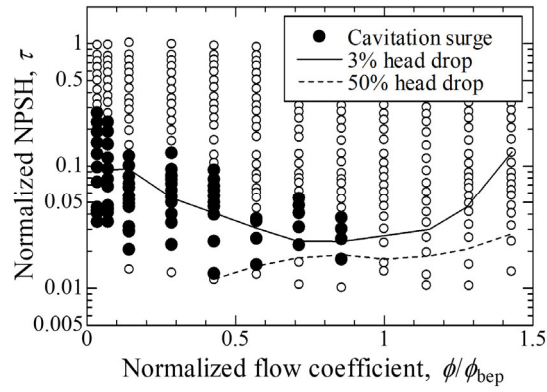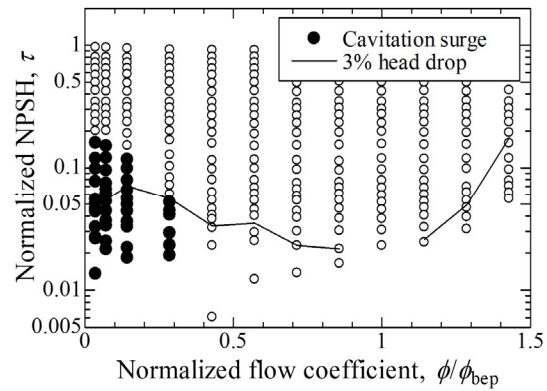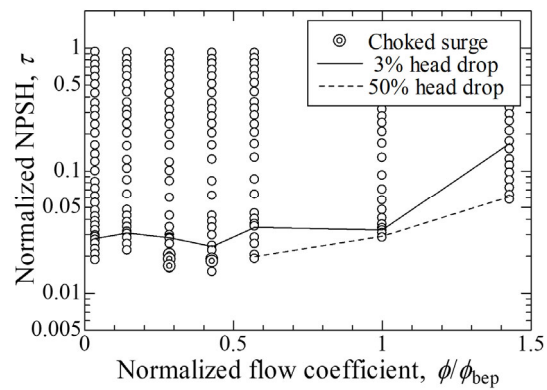(a) Straight casing   (b) RSP62   (c) RSP62 with SB

Fig. 15 Typical examples of FFT analyses of upstream (top) and downstream (middle) pressure fluctuations along with head breakdown curve (bottom). Normalized flow rate is $\phi/\phi_{\text{bep}} = 0.29$. (i) denotes onset range of cavitation surge, while (ii) denotes choked surge which occurs during head degradation.

(a) Straight casing

(b) RSP62 only

(c) RSP62 with SB
Fig. 16 Onset region of cavitation surge with/without suppression device

Table 1 Specifications of model inducer

Number of blades, Z_i	4
Tip diameter, D_t [mm]	64
Inlet hub ratio, D_{h1}/D_t	0.38
Outlet hub ratio, D_{h2}/D_t	0.55
Inlet tip blade angle, β_{t1} [deg.]	7.00
Outlet tip blade angle, β_{t2} [deg.]	16.85
Tip clearance ratio, c/D_t	0.0078

Table 2 Number of computational nodes

	Casing geometry	No. of nodes
(i)	Straight casing	About 1.02M
(ii)	Circumferential groove with SB	About 4.47M
(iii)	RSP (D'/D_c=0.89)	About 0.96M
(iv)	RSP (D'/D_c=0.78)	About 0.92M
(v)	RSP (D'/D_c=0.89) and SB (h=0.02D_t)	About 1.04M
(vi)	RSP (D'/D_c=0.89) and SB (h=0.04D_t)	About 1.04M
(vii)	RSP (D'/D_c=0.89) and SB (h=0.06D_t)	About 1.04M
(viii)	RSP (D'/D_c=0.78) and SB (h=0.02D_t)	About 0.97M

Table 3 Results of unsteady analyses normalized by those of steady analyses

Flow coefficient	0.012	0.074
Head	0.98	0.97
Shaft power	0.97	0.98
Efficiency	1.0	0.99
Back flow rate	0.99	1.0

Table 4 Specification of test pump

Inducer	
Number of blades, Z_i	3
Inlet hub-to tip ratio, D_{h1}/D_t	0.38
Outlet hub-to tip ratio, D_{h2}/D_t	0.57
Tip clearance ratio, c/D_t	0.003
Main impeller	
Number of blades, Z_m	15
Inner/outer diameter ratio, D_{m1}/D_{m2}	0.29
Outlet blade height ratio, b_{m2}/D_{m2}	0.074
Outlet blade angle, β_{mb2}[deg.]	30